International Journal of Environmental Science and Technology (2020) 17:2401–2414
https://doi.org/10.1007/s13762-019-02554-6

ORIGINAL PAPER

Experimental investigation of a heat pump-assisted solar humidification–dehumidification desalination system with a free-flow solar humidifier

M. Shojaei[1] · H. Mortezapour[1] · K. Jafarinaeimi[1]

Received: 10 April 2019 / Revised: 4 August 2019 / Accepted: 25 September 2019 / Published online: 3 October 2019

Abstract

Global water scarcity is one of the biggest human concerns in recent decades. Seawater desalination becomes the dominant way to access the new drinkable waters. The present study developed a heat pump-assisted humidification–dehumidification water desalination system. The designed system is equipped with a novel solar humidifier that works based on the free-flow solar water collectors. The effect of air flow rate and mode of the air circulation system on the performance of the designed system was experimentally investigated. The results reveal that raising the air flow rate improved water evaporation rate and the solar humidifier efficiency, while closing the air circuit led to a reduction in the evaporation rate. The maximum evaporation amount and water productivity were around 1.38 and 1 kg/h/m^2 in the average solar irradiance of 877 W/m^2. The closed-loop air circulation system resulted in a significantly higher effectiveness of dehumidification and produced higher desalinated water compared with the open-circuit mode. The lowest specific electrical energy consumption and the highest gained output ratio values of, respectively, 0.15 kWh/kg and 2.36 were observed at the air flow rate of 0.019 m^3/s/m^2 of solar humidifier when closing the air circulation system.

Keywords Evaporation rate · Productivity · Air circulation · Specific energy consumption · Gained output ratio

List of symbols

A	Surface area (m^2)
a	Accuracy
E	Electrical energy (kWh)
G	Solar irradiance (W/m^2)
GOR	Gained output ratio (decimal)
H	Specific enthalpy (J/kg)
L	Latent heat (J/kg)
M	Mass of desalinated water (kg)
$\dot{m}$	Mass flow rate (kg/s)
PCF	Pre-condenser fraction (decimal)
$\dot{Q}$	Rate of useful energy gain (W)
SEEC	Specific electrical energy consumption (kWh/kg)
T	Temperature (°C)
U	Overall heat loss coefficient of solar collector (W/m^2/°C)
u	Uncertainty
x	Measured parameter
y	Calculated parameter

Greek letters

α	Absorption coefficient of absorber plate (decimal)
ζ	Thermal efficiency (%)
ε	Effectiveness (decimal)
τ	Transmission coefficient of glass cover (decimal)
ω	Absolute humidity (kg moisture/kg air)

Subscripts

a	Air
amb	Ambient
b	Brine
c	Condensation
DH	Dehumidification
EC_o	Outlet of evaporative condenser
EC_i	Inlet of evaporative condenser
el	Electrical
HE_i	Inlet of heat pump evaporator
HE_o	Outlet of heat pump evaporator

Editorial responsibility: M. Abbaspour.

H. Mortezapour
h.mortezapour@uk.ac.ir

[1] Department of Biosystems Engineering, Faculty of Agriculture, Shahid Bahonar University of Kerman, Kerman, Iran

P	Absorber plate
PC_o	Outlet of pre-condenser
r	Refrigerant
SC	Solar collector
SC_i	Inlet of solar collector
th	Thermal
v	Vaporization
w	Seawater

Introduction

Global water scarcity has become one of the biggest human concerns in recent decades. Less than 2.6% of the total water on the earth is fresh, from which only 30% is usable by human (Barlow and Clarke 2017). At least 30% of people throughout the world suffer from water scarcity. Climate changes, natural disasters, rapid population, economic growth, and accelerated urbanization are some of the factors influencing accessibility to freshwater (Lawal et al. 2018; WWAP 2012). Besides the management of the existing water resources, desalination is becoming the dominant approach to access the new drinkable water. Both thermal and membrane desalination plants consume a large amount of energy (Moumouh et al. 2014). The economic and environmental consequences of fossil fuel spurred growing interest in the use of renewable energies as the alternative or supplementary to fossil fuel resources. Numerical modeling of an advanced biological wastewater treatment plant was carried out, and the obtained results were confirmed by the experimental data. A 2.85 MW photovoltaic (PV) generator was also considered to meet the energy requirement of the plant with the daily capacity of 134.9 ML wastewater. The study concluded that the performance of the proposed plant could be improved by employing solar thermal energy and geothermal heat pump to control the wastewater temperature (Gürtekin 2019).

Among the thermal-based desalination techniques, the humidification–dehumidification (HDH) of air, due to the ability for operation at low temperature and use renewable energies as the heat source, is known as a simple method especially suited for regions in developing countries (Santosh et al. 2019). Solar collectors were widely employed in the HDH systems where they heat water to humidify the circulating air. Dehumidification of the humid air to produce freshwater is accomplished by cooling down the air below the dew point. The analysis results of an open-type solar-assisted HDH system indicated that the temperature of the water, air, and glass cover, as the condenser, significantly influenced the productivity of freshwater. Maximum productivity of 2.2 kg/m^2/day was reported in this study (Hammadi 2018). Zarzoum et al. (2016) have numerically studied an HDH-based solar desalination system to investigate the influence of the meteorological and operating parameters, including the inlet temperature of air and water as well as the air flow rate, on the system productivity. El-Said et al. (2016) have investigated the use of nano-fluid solar water heaters to heat the saline water in a two-stage HDH desalination system. A maximum solar water heater efficiency of 49.4% and a gained output ratio of 7.5 was achieved in this research. An HDH desalination system was equipped with a concentrated photovoltaic-thermal air collector (surface area of 9 m^2) for simultaneous production of freshwater and electricity. The annual freshwater capacity of the system was around 12 m^3, and the cost of freshwater production was estimated to be 0.01$/L (Elsafi 2017).

To improve the energy efficiency of the HDH systems, some configurations were designed to recover the condensation heat and reutilize for air or water heating in the humidification process. In this way, heat pump technology has been widely employed in desalination systems. Zhang et al. (2018) have experimentally studied an HDH system with the heat pump unit and reported maximum water productivity of 22.26 kg/h, and an estimated cost of 0.051 $/kg of produced water. Dehghani et al. (2018) developed a mathematical model to describe the performance of an HDH system coupled with a heat pump under different working conditions. An optimum specific electrical energy consumption of 335.4 kWh/m^3 was achieved in this research. Numerical investigation of a heat pump-assisted HDH desalination system was carried out by Zhang et al. (2019). The results showed that the air temperature had no significant effect on productivity, while the increase in the relative humidity caused an improvement in freshwater production. The average production cost of 0.0412$/L was reported in this study. A novel configuration for the heat pump-assisted HDH seawater desalination systems was proposed by He et al. (2018), in which the evaporator was employed to recycle the accumulated heat in the discharging brine and deliver to the condenser for heating the seawater. Rostamzadeh et al. (2018) achieved the maximum gained output ratio of 9.02 using an HDH system equipped with absorption-compression heat pump cycle that recovered waste heat of brine.

Most of the HDH desalination systems utilize the water spraying technology to achieve a suitable evaporation rate in the humidification process (El-Agouz et al. 2014). Rahimi-Ahar et al. (2018) proposed an HDH system with a vacuum humidifier. The results revealed that reducing the humidifier pressure significantly increased the desalinated water production. Gao et al. (2008) developed an HDH system, in which the humidification was accomplished by spraying the seawater on an alveolate humidifier. Xu et al. (2019) compared two kinds of humidifying packing materials, including plastic polyhedron empty balls (PPEBs) and honeycomb paper in a solar-assisted heat pump desalination system. The study showed that using the PPEBs resulted in more improvement in the system productivity at the same condition of the air flow rate because of the greater specific surface area.

In a research, Zondag et al. (2003) studied different configurations of hybrid solar water collectors and concluded that although the free-flow concept provides suitable heat gain from the absorber panel and presents a fair thermal efficiency, it is not a good choice for use in the solar water heaters due to the strong water evaporation rate especially at the higher temperatures. To use the suitable water evaporation potential of the free-flow water collectors, the present study attempted to develop a novel heat pump-assisted solar HDH desalination system with a combined water sprayer-free-flow solar humidifier. Although a large number of solar-assisted HDH desalination systems are presented in the literature, integration of solar collector and humidifier in a single part has not been investigated, so far. The performance of the designed system was experimentally investigated under different air flow rates and two modes of the air circulation system including closed-loop and open-circuit. The tests were carried out during June 2018 in Kerman, Iran.

Materials and methods

Setup description

The designed water desalination system includes a water pump, seawater tank, solar humidifier, distribution pipe, water sprayers, pre-condenser, evaporative condenser, blower, and heat pump unit, as indicated in Fig. 1. The water pump transfers the seawater from the tank to the distribution pipe installed on the top end of the flat plate absorber of the solar collector that works as the humidifier. A part of the water is evaporated when moving down over the absorber plate under the influence of direct contact with the hot plate and the heated air. The water vapors, involved in the airflow, pass through a heat exchanger, which is located after the solar collector and works as the pre-condenser. In the pre-condenser, a part of the energy of the humid air is transferred to the seawater flow entering the humidifier. This reduces the airflow temperature, hence, facilitates the water condensation, and preheats the seawater flow before the humidifier. The increase in the seawater temperature enhances the kinetic energy of the water molecules, which leads to improvement in the evaporation rate during the humidification process. The evaporative condenser is made of a helical tube vertically installed in a tank filled with water, as the heat storage material. The heat pump evaporator is also located in the tank to provide the cooling load needed for the dehumidification. The helical tube is ended into the desalinated water container. A return duct, connected to the container, leads back the airflow to the inlet of the system, where the heat pump condenser preheats the air before the solar collector. To supply the electrical energy needed for the blower, pump, and heat pump compressor independently of the grid, a stand-alone photovoltaic system including photovoltaic module, battery, charge controller, and inverter was installed beside the water desalination system.

Photographs of the desalination system are shown in Fig. 2. The blower was installed before the heat pump condenser to circulate the air through the system components.

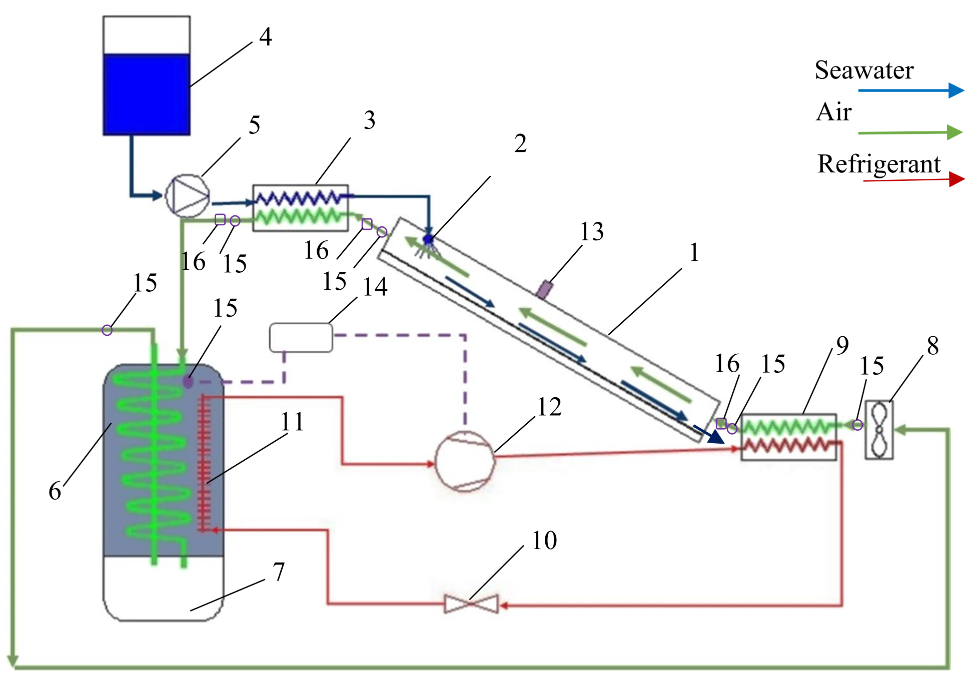

Fig. 1 Schematic sketch of the desalination system and location of the measurement instruments: 1—solar humidifier, 2—water sprayer, 3—pre-condenser, 4—seawater tank, 5—water pump, 6—evaporative condenser, 7—desalinated water, 8—blower, 9—heat pump condenser, 10—expansion valve, 11—heat pump evaporator, 12—compressor, 13—pyranometer, 14—temperature controller, 15—temperature sensor, 16—RH sensor

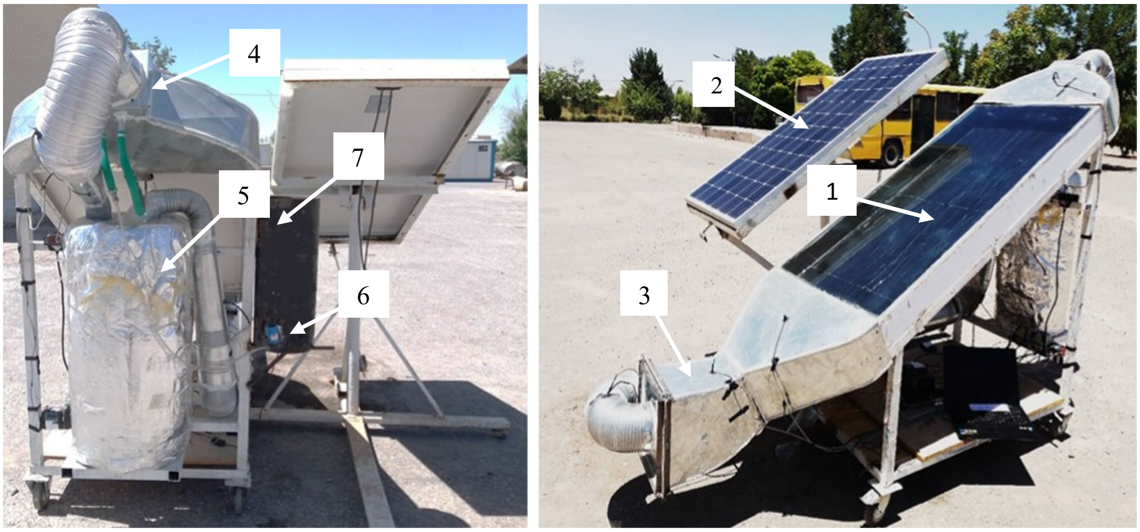

Fig. 2 The designed heat pump-assisted solar HDH desalination system: 1—solar humidifier, 2—photovoltaic module, 3—blower and condenser housing, 4—pre-condenser housing, 5—evaporative condenser, 6—seawater pump, 7—seawater tank

The water pump provided a steady seawater flow to the humidification unit. The flat plate absorber in the solar humidifier was a black painted aluminum sheet installed in a wooden duct whose sides were thermally insulated using a glass wool cover. The pre-condenser, as a cross-flow heat exchanger, had an adequate total surface area to reach the leaving humid air from the humidifier with the average flow rate of 0.014 $m^3/s/m^2$ (at the average temperature of 55 °C and RH of 65% observed in the pre-experiments) to the dew point condition, assuming a seawater flow rate of 2.5 L/min with the average temperature of 20 °C. It was a finned-tube aluminum heat exchanger with the outer dimensions of $0.170 \times 0.170 \times 0.040$ m.

The helical tube in the construction of the evaporative condenser had a total length of 2.300 m and diameter of 0.080 m to provide a cooling load of 630 W to achieve an average condensation rate of 1 kg/h, considering an average temperature of 20 °C for the surrounding heat storage material. The tube was located in the water tank constructed from stainless steel material with a diameter of 0.670 m. A glass wool sheet of thickness 0.025 m was used for thermal insulation of the tank. The freshwater container was separated from the condenser tank using a stainless sheet.

The heat pump system was comprised of the condenser, compressor, expansion valve, and evaporator. Tetrafluoroethane that is known as R134a, from the family of hydrofluorocarbons (HFC), was utilized as the refrigerant in the heat pump system. The heat pump condenser was a finned-tube aluminum heat exchanger with 58 fins, and a helical copper pipe was used as the heat pump evaporator in the water tank of the dehumidification unit.

The photovoltaic system was employed to supply the electrical energy needed for the pump, blower, and heat pump compressor. The PV system was designed to supply the electrical energy needs of the desalination system to work at least 6 h per day of summer in Kerman city, Iran. Technical specifications of the different components of the designed HDH desalination system are given in Table 1.

Mathematical models of the humidification and dehumidification

The following assumptions were considered for the mathematical modeling of the humidifier and dehumidifier units:

- The system is in a steady-state condition.
- Heat losses from the dehumidifier to the ambient air are neglected.
- Kinetic and potential energies are not taken into calculations.

The mass and energy balance equations of the humidifier can be given as:

$$\dot{m}_{\mathrm{w}} - \dot{m}_{\mathrm{b}} = \dot{m}_{\mathrm{v}} = \dot{m}_{\mathrm{a}}\left(\omega_{\mathrm{a\_SC\_o}} - \omega_{\mathrm{a\_SC\_i}}\right) \quad (1)$$

$$\dot{m}_{\mathrm{b}}H_{\mathrm{b}} - \dot{m}_{\mathrm{w}}H_{\mathrm{w}} + \dot{m}_{\mathrm{a}}\left(H_{\mathrm{a\_SC\_o}} - H_{\mathrm{a\_SC\_i}}\right) = A_{\mathrm{SC}}\left[G\tau\alpha - U\left(T_{\mathrm{p}} - T_{\mathrm{amb}}\right)\right] \quad (2)$$

where $\dot{m}_{\mathrm{a}}$, $\dot{m}_{\mathrm{w}}$ and $\dot{m}_{\mathrm{b}}$ stand for the mass flow rates of, respectively, the air, seawater and brine (kg/s); $\dot{m}_{\mathrm{v}}$ is the moisture evaporation rate in the humidifier (kg/s); $\omega_{\mathrm{a\_SC\_o}}$ and $\omega_{\mathrm{a\_SC\_i}}$ are the absolute humidities of the moving air at the outlet and inlet of the humidifier (kg moisture/kg air), respectively;

Table 1 Technical specifications of the different components of the system

Component	Technical specification
Blower	12 V—DC, nominal input power: 45 W
Seawater pump	12 V—DC, nominal input power: 12 W
Solar humidifier	Absorber: black painted aluminum sheet, total surface area: 1.2 m^2, transparent cover: glass sheet, thickness: 6 mm
Pre-condenser	Type: finned-tube heat exchanger, material: aluminum, total surface area: 1.050 m^2
Evaporative condenser	Type: helical tube, length: 2.300 m, diameter: 0.080 m
Heat pump	Compressor: scroll type, input power: 90 W, cooling capacity: 330 W; evaporator: helical pipe, material: copper, length: 2.000 m, diameter: 0.008 m; condenser: finned-tube heat exchanger, material: aluminum, number of fins: 58, outer dimensions: $0.240\times0.220\times0.050$ m; expansion valve length: 3.3 m, inner diameter: 0.78×10^{-3} m
PV system	Maximum power of PV module: 180 W; charge controller: 12/24 V with the maximum current of 30 A; battery capacity: 86 Ah; rating power of DC to Ac inverter: 350 W

H_{b}, H_{w}, $H_{\mathrm{a\_SC\_o}}$, and $H_{\mathrm{a\_SC\_i}}$ show the specific enthalpies of, respectively, the brine, seawater, inlet and outlet air of the solar collector (J/kg); A_{SC} is the surface area of the solar collector (m^2); G stands for the solar radiation on the collector (W/m^2); τ and α are the transmission coefficient of the glass cover and the absorption coefficient of the absorber plate, respectively; U is the overall heat loss coefficient of the solar collector (W/m^2/°C); T_{p} and T_{a} are the temperatures of the absorber plate and the ambient air (°C), respectively.

The corresponding mass and energy equations for the dehumidifier can be written as:

$$\dot{m}_{\mathrm{c}} = \dot{m}_{\mathrm{a}}\left(\omega_{\mathrm{a\_EC\_o}} - \omega_{\mathrm{a\_EC\_o}}\right) \tag{3}$$

$$\dot{m}_{\mathrm{r}}\left(H_{\mathrm{r\_HE\_i}} - H_{\mathrm{r\_HE\_o}}\right) = \dot{m}_{\mathrm{a}}\left(H_{\mathrm{a-EC\_i}} - H_{\mathrm{a-EC\_o}}\right) \tag{4}$$

where $\dot{m}_{\mathrm{c}}$ is the vapor condensation rate in the dehumidifier (kg/s); $\omega_{\mathrm{a\_EC\_o}}$ and $\omega_{\mathrm{a\_EC\_o}}$ show the absolute humidities of the air at the inlet and outlet of the evaporative condenser, respectively (kg moisture/kg air); $\dot{m}_{\mathrm{r}}$ stands for the mass flow rate of the refrigerant (kg/s); $H_{\mathrm{r\_HE\_i}}$ and $H_{\mathrm{r\_HE\_o}}$ show the specific enthalpies of the refrigerant at the inlet and outlet of the heat pump evaporator, respectively (J/kg); $H_{\mathrm{a\_EC\_o}}$ and $H_{\mathrm{a\_EC\_i}}$ are the specific enthalpies of the air at the outlet and inlet of the evaporative condenser, respectively (J/kg).

Experimental procedure

The experimental tests were carried out during June 2018 in Kerman, Iran. Each trial started at 10:30 a.m. and continued until 12:30 p.m. The tests were conducted at the different air flow rates of 0.009, 0.014, and 0.019 m^3/s/m^2 of solar humidifier that were selected by trials and two modes of the air circulation system including open-circuit and closed-loop. At the mode of open circuit, the humid air, after passing through the dehumidification unit, was discharged to the ambient, and instead of it, fresh air entered into the system. The seawater flow rate kept constant (around 2.5 L/min) for all tests, and the average temperature of the seawater tank was around 23.2 ± 3 °C during the experiments. Inlet and outlet temperatures and relative humidity of the solar humidifier, pre-condenser, evaporative condenser, as well as the heat pump condenser, were measured by time intervals of 15 min. Furthermore, the required power of the heat pump compressor, blower, and water pump was recorded every 0.5 s during the tests. Ambient condition data, including temperature, relative humidity, and solar irradiance on the solar collector surface were also recorded by time intervals of 15 min.

Performance parameters

Performance evaluation of the designed desalination system was conducted based on the parameters of thermal efficiency of solar humidifier, effectiveness of dehumidification, pre-condenser fraction, specific electrical energy consumption, and gained output ratio. Thermal efficiency and evaporation rate were the key parameters to investigate the performance of the solar collector as the humidifier. Thermal efficiency of the collector was defined as follow:

$$\zeta_{\mathrm{th}} = \frac{\dot{Q}_{\mathrm{SC}}}{GA_{\mathrm{SC}}} \times 100 \tag{5}$$

where ζ_{th} is thermal efficiency (%), and $\dot{Q}_{\mathrm{SC}}$ is the rate of useful energy gain by the solar collector (W). The following expression gives the rate of useful energy gain by the solar collector.

$$\dot{Q}_{\mathrm{SC}} = \dot{m}_{\mathrm{a}}\left(H_{\mathrm{a\_SC\_o}} - H_{\mathrm{a\_SC\_i}}\right) \tag{6}$$

Moisture evaporation rate ($\dot{m}_{\mathrm{v}}$) was determined based on Eq. 1 using the air mass flow rate and the absolute humidities of the air at the inlet and outlet of the solar collector. Condensation rate ($\dot{m}_{\mathrm{c}}$) in the dehumidification unit was obtained from Eq. (3) by measuring the absolute humidities of the inlet and outlet air of the dehumidifier.

Since the dehumidification unit was designed to separate all of the moisture added to the moving air along the humidification unit, its effectiveness was defined based on the expression developed by Xu et al. (2019):

$$\varepsilon_{DH} = \frac{\omega_{a\_SC\_o} - \omega_{a\_EC\_o}}{\omega_{a\_SC\_o} - \omega_{amb}} \tag{7}$$

where ε_{DH} shows effectiveness of dehumidification (decimal) and ω_{amb} is the absolute humidity of the ambient air (kg moisture/kg air).

A useful parameter that was used to determine the role of the pre-condenser in the vapor condensation during the dehumidification process is pre-condenser fraction (PCF). In other words, PCF describes the contribution of absorbed energy from the moving air by the pre-condenser, in both terms of sensible and latent heat, to total energy reduction in the dehumidification unit. The following expression was used to calculate PCF.

$$\mathrm{PCF} = \frac{H_{a\_SC\_o} - H_{a\_PC\_o}}{H_{a\_SC\_o} - H_{a\_EC\_o}} \tag{8}$$

where $H_{a\_PC\_o}$ and $H_{a\_EC\_o}$ are the outlet specific enthalpies (J/kg) of the pre-condenser and evaporative condenser, respectively.

Specific electrical energy consumption (SEEC), in kWh/kg, was obtained using the following expression (Dehghani et al. 2018).

$$\mathrm{SEEC} = \frac{E_{el}}{M} \tag{9}$$

where E_{el} is the electrical energy used by the water pump, blower, and heat pump compressor (kWh) and M stands for the amount of produced desalinated water (kg).

Another useful parameter that describes the quality of thermal energy use of the system is gained output ratio (GOR), which was calculated as follow (Dehghani et al. 2018; Rajaseenivasan et al. 2016):

$$\mathrm{GOR} = \frac{\dot{m}_c L_v}{\dot{Q}_{SC}} \tag{10}$$

where L_v is latent heat of vaporization of water (J/kg).

Instrumentation and uncertainty analysis

Technical specification of the instruments used during the experiments is shown in Table 1. To determine the uncertainty of the instruments ($u(x)$), the following expression was used (Rahbar and Esfahani 2012; Zhang et al. 2018);

$$u(x) = \frac{a}{\sqrt{3}} \tag{11}$$

where a is the accuracy of the instrument. The uncertainty of the calculated parameters was estimated by (Sardouei et al. 2018; Sözen et al. 2018):

$$u(y) = \left[\sum \left(\frac{\partial y}{\partial x_i} u(x_i) \right)^2 \right]^{1/2} \tag{12}$$

where y is the calculated parameter and x stands for the measured parameter. Tables 2 and 3 provide the estimated uncertainties of the instrument and the calculated parameters, respectively.

Results and discussions

Variation of ambient conditions

Variations of solar radiation intensity and the ambient temperature between 10:30 a.m. and 12:30 p.m. in a typical day of experiments on May 2018 are depicted in Fig. 3. Ambient

Table 3 Results of uncertainty analysis of the calculated parameters

No.	Parameter	Uncertainty
1	Thermal efficiency of solar collector	±1.72%
2	Moisture evaporation rate	±0.0006 kg/s
3	Effectiveness of dehumidification unit	±2.1%
4	Specific electrical energy consumption	±0.025 kWh/kg
5	Gained output ratio	±2.3%

Table 2 Technical specification and results of uncertainty analysis of the instruments

No.	Instrument (model)	Measured parameter	Accuracy	Range	Uncertainty
1	Temperature sensor (SMT 160)	Air temperature	±0.7 °C	−30 to 130 °C	0.4 °C
2	RH sensor (SUN25-H)	RH of air	±3%	0–100%	1.73%
3	Pyranometer (TES1333)	Solar irradiance	±1 W/m^2	0–2000 W/m^2	0.58 W/m^2
4	Switched temperature controller (STC-100)	Water temperature	±1 °C	−40–99 °C	0.58 °C
5	Anemometer (TES1340)	Air velocity	±0.3 m/s	0–30 m/s	0.17 m/s
6	Wattmeter (TM1510)	Electrical power consumption	±0.1 W	40 mA–5 A 50–500 V	0.058 W

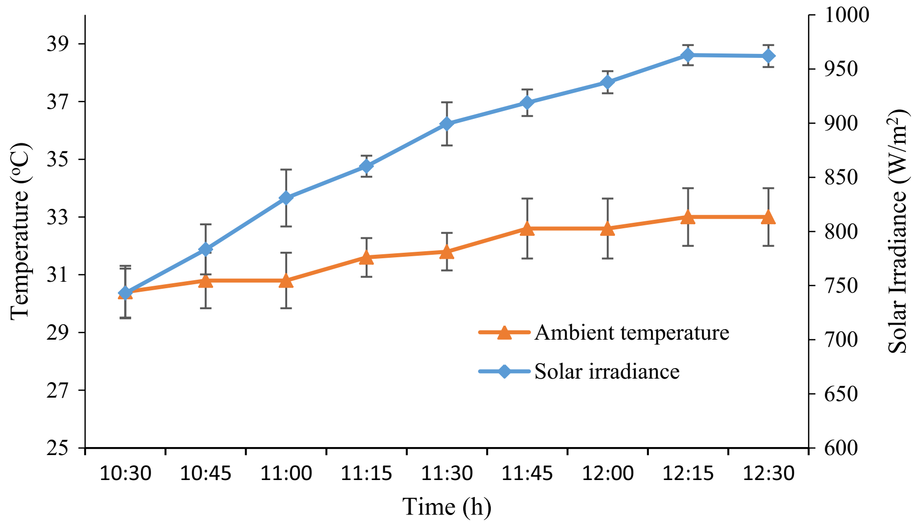

Fig. 3 Variations of solar irradiance and ambient temperature during the experiments

temperature varied between 29.8 and 33.0 °C. The maximum solar irradiance on the collector surface was around 963 W/m^2, measured at 12:15 afternoon. The average values of ambient temperature and solar radiation during the tests were 31.8 ± 1 °C and 877 ± 111 W/m^2, respectively.

Performance of humidification unit

Variations of temperature and RH of the moving air at the humidifier outlet are illustrated in Figs. 4 and 5, respectively. The outlet temperature increased with the time that is attributed to the growth of the ambient temperature and solar irradiance. Furthermore, raising the air flow rate from 0.009 to 0.019 m^3/s/m^2 slightly increased the outlet temperature. This was because of the enhancement in the convection coefficient of the moving air that increases the heat gain from the solar collector (Bergman and Incropera 2011). Figure 4 also demonstrates that the outlet temperature raised when the air circulation system was closed. This was owing to the higher temperature of the air at the humidifier inlet with the closed-loop system. In contrast with temperature, relative humidity of the air slightly decreased with increasing the air flow rate. This reveals the fact that the absolute humidity of the air leaving the humidification unit may be reduced due to faster moving through the solar collector. Furthermore, it can be understood that the leaving air from the dehumidification unit, which moves back to the humidifier when the air system is closed, has a significantly higher temperature and RH compared with the fresh ambient air that enters to the humidifier at the open-circuit air system. This large initial deviation makes that the outlet temperature and RH of the humidifier remain slightly higher at the mode of the closed-loop system.

Cumulative water evaporation in the solar humidifier during the tests is indicated in Fig. 6. Raising the air flow rate caused an increment in the evaporation rate mainly because of the increase in the heat and mass transfer coefficients of the air at the higher velocities. It can be indicated based on the calculations that the average evaporation rate increased by 23% when the air flow rate increased from 0.009 to 0.019 m^3/s/m^2. Similar results were obtained by Zarzoum et al. (2016). The calculations also show a reduction of 25% in the evaporation amount with closing the air circulation system. The reason is the higher vapor pressure of the airflow at the vicinity of the water layer, due to its higher RH, that reduces the water diffusion rate to the air. A similar result was reported by Akhatov et al. (2016).

Thermal efficiency of the solar humidifier at the different operating conditions of the desalination system is illustrated in Fig. 7. Clearly, the efficiency improved with opening the air circulation system and raising the air flow rate due to the enhancement of the evaporation rate. Similarly, Rajaseenivasan et al. (2016) reported an increment in the humidifier efficiency of an HDH desalination system coupled with the solar collectors when increasing the air flow rate. This is also in agreement with the results of El-Agouz (2010). It can be noticed from Fig. 7 that thermal efficiency of the solar humidifier ranged from 40 to 92%, and the highest efficiency was measured at the air flow rate of 0.019 m^3/s/m^2 when the air circulation system was open. Zondag et al. (2003) achieved a thermal efficiency of 62% for the free-flow photovoltaic-thermal collector.

Performance of dehumidification unit

Cumulative desalinated water during the tests is shown in Fig. 8. The condensation rate in the dehumidification unit depends on the rate of heat transfer, the residence time of the air in the condenser and dew point temperature of the air. The closed-loop air circulation system achieved a

Fig. 4 Variations of the outlet temperature of the collector

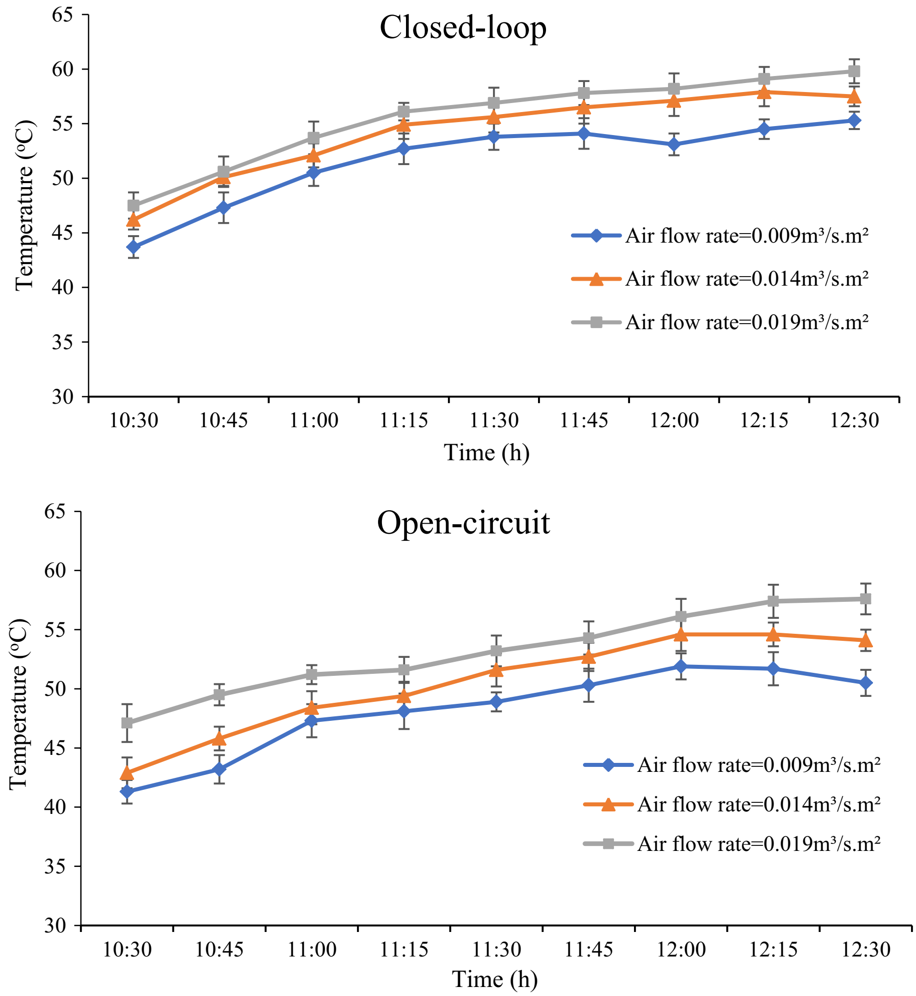

significantly higher condensation rate compared with the open-circuit mode because of the higher humidity and consequently, the higher dew point of the moving air. Raising the air flow rate, on the one hand, slightly increases the air temperature and the heat transfer coefficient, but on the other hand, shortens the residence time in the condenser that leads to a decrease in the condensation rate (Eid et al. 2018). For these reasons, raising the air flow rate, at the closed-loop air system, led to a slight increment in freshwater production, while at the open-circuit mode, it resulted in declination in the productivity. Gao et al. (2008) and Ghazy and Fath (2016) indicated productivity improvement with the increase of the air flow rate. However, a maximum amount of desalinated water of around 2.41 kg (productivity of 1.00 kg/m^2/h) was achieved at the maximum air flow rate when the air circulation system was closed. Hammadi (2018) and Rahimi-Ahar et al. (2018) reported the water productivities of 4.92 L/m^2/day, 2.2 kg/m^2/day, and 1.07 L/m^2/h, respectively.

Effectiveness of the dehumidification unit and the pre-condenser fraction at the different operating conditions are shown in Figs. 9 and 10, respectively. The closed-loop had higher effectiveness compared with the open-circuit air system as the calculation reveals that the effectiveness increased by ten times, on average, when closing the air circulation system. A slight increment in the effectiveness was also observed when raising the air flow rate from 0.009 to 0.019 m^3/s/m^2 at the closed-loop mode of the air circulation system, while it decreased the effectiveness at the open-circuit mode. The maximum dehumidification effectiveness was around 0.94 at the air flow rate of 0.019 m^3/s/m^2 with the closed-loop air system. Liu and Sharqawy (2016) observed the effectiveness of below 0.94 with a bubble column humidifier and dehumidifier, in which the dehumidification carried out under elevated pressures. Kabeel et al. (2014) achieved the effectiveness value of 0.71 using a liquid–gas heat exchanger as the dehumidifier.

The pre-condenser fraction values were ranged from 3.5 to 9.6%, and the maximum value was observed at the flow rate of 0.009 m^3/s/m^2 with opening the air circulation system. Since effectiveness of the dehumidification unit and especially the evaporative condenser was higher with

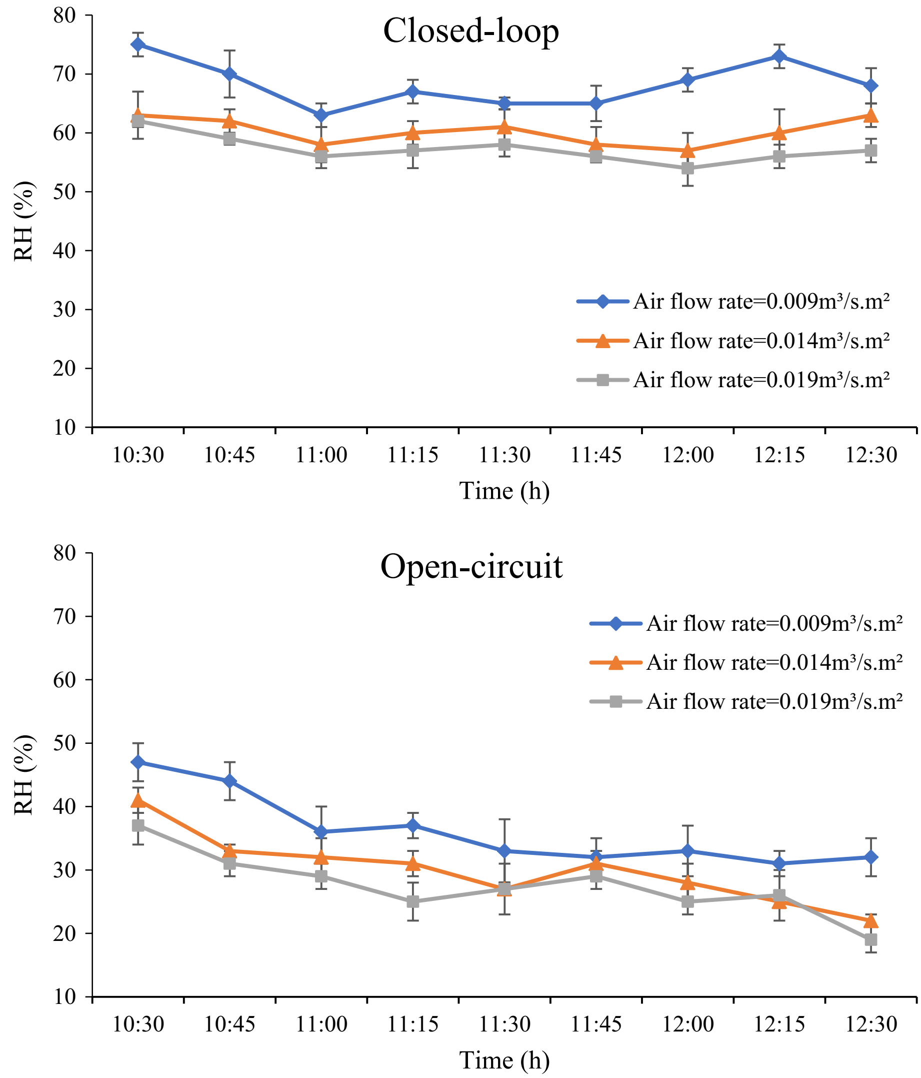

Fig. 5 Variations of RH of the air at the collector outlet

the closed-loop air system, the PCF values significantly declined when the air system was closed.

Variation in specific electrical energy consumption of the system is illustrated in Fig. 11. The observation shows that SEEC decreased by 70% by using the closed-loop air circulation system. This occurred mainly because of the higher effectiveness of the dehumidification unit at the closed-loop mode. With the same reason, at the open-circuit air system, decreasing the mass flow rate to 0.009 $m^3/s/m^2$ reduced the electrical energy consumption by 43%. Unlike with the open system, SEEC slightly reduced with raising the flow rate when using the closed-loop system. The minimum value of SEEC was found to be around 0.15 kWh/kg, observed at the flow rate of 0.019 $m^3/s/m^2$ with employing the closed-loop mode of the air system. Dehghani et al. (2018) achieved a SEEC of 260–370 kWh/m^3 using a heat pump-driven HDH desalination system. Investigation of a mechanical vapor compression desalination system showed a minimum specific energy consumption value of 9.8 kWh/m^3 (Jamil and Zubair 2017).

Variation of the average GOR values at the different operating conditions of the HDH system is shown in Fig. 12. It can be noticed that the GOR values had a significant increment when using the closed-loop compared with the open-circuit air system. The maximum GOR was about 2.36 at the air flow rate of 0.019 $m^3/s/m^2$ and the closed-loop mode of the air circulation system. Elminshawy et al. (2016) and Xu et al. (2018) reported the GOR values of 3.15 and 1.93, respectively.

Fig. 6 Cumulative water evaporation in the solar humidifier during the tests

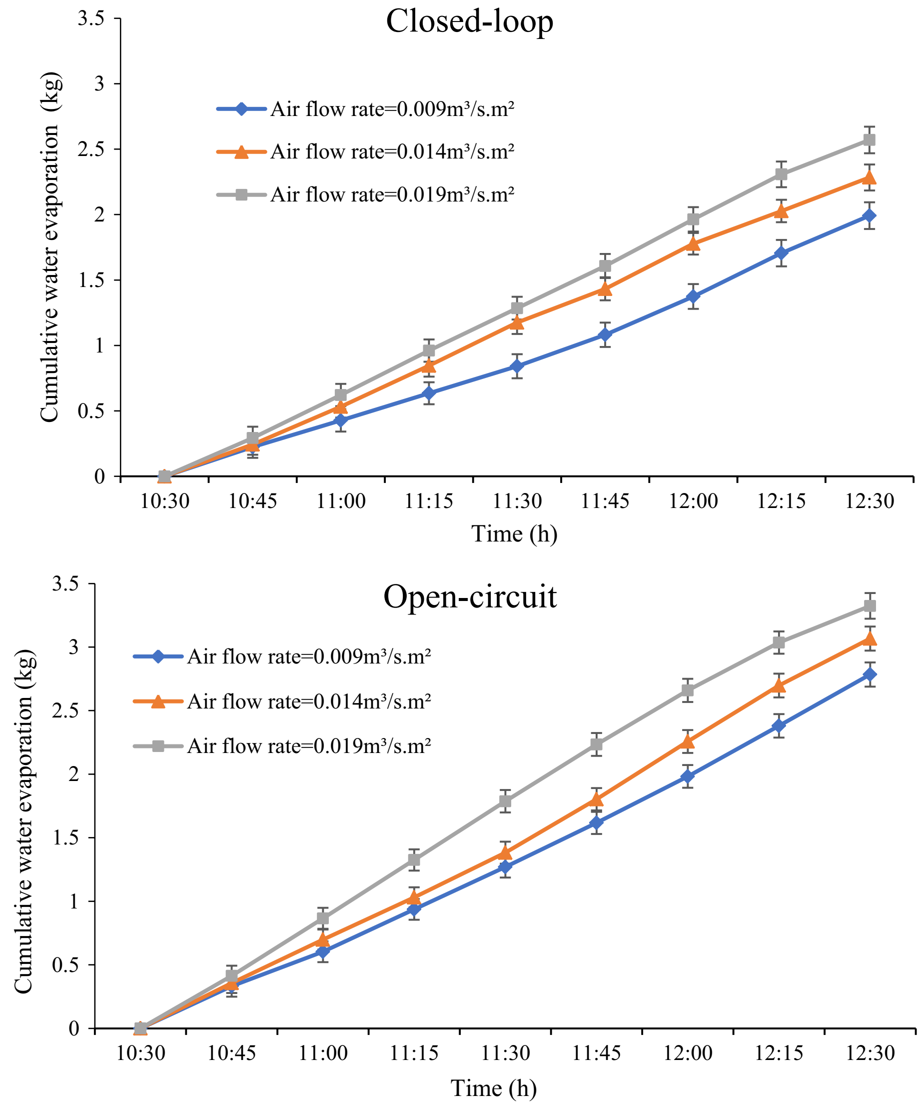

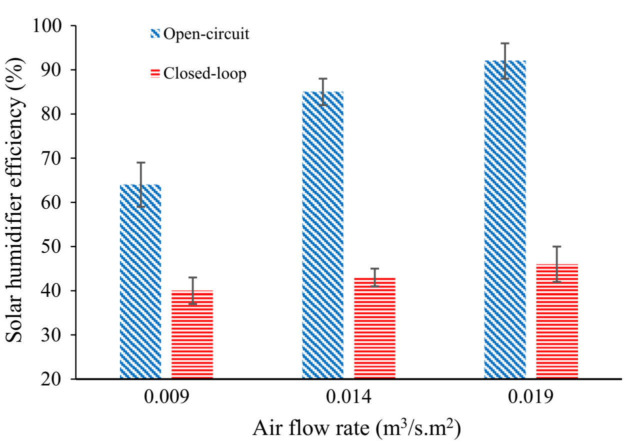

Fig. 7 Variation of thermal efficiency of the solar humidifier

Conclusion

The present study developed a heat pump-assisted humidification–dehumidification solar water desalination system with a free-flow solar humidifier. The effect of air flow rate and mode of the air circulation system on the performance of the designed system was experimentally investigated. The results can be summarized as follow:

- Increasing the air flow rate improved water evaporation rate and the solar humidifier efficiency, while closing the air circuit led to a reduction in the evaporation rate.
- The average effectiveness of dehumidification was significantly improved when applying the closed-loop instead of the open-circuit air circulation system and maximum effectiveness of 94% was achieved during the experiments.

Fig. 8 Cumulative desalinated water produced during the tests

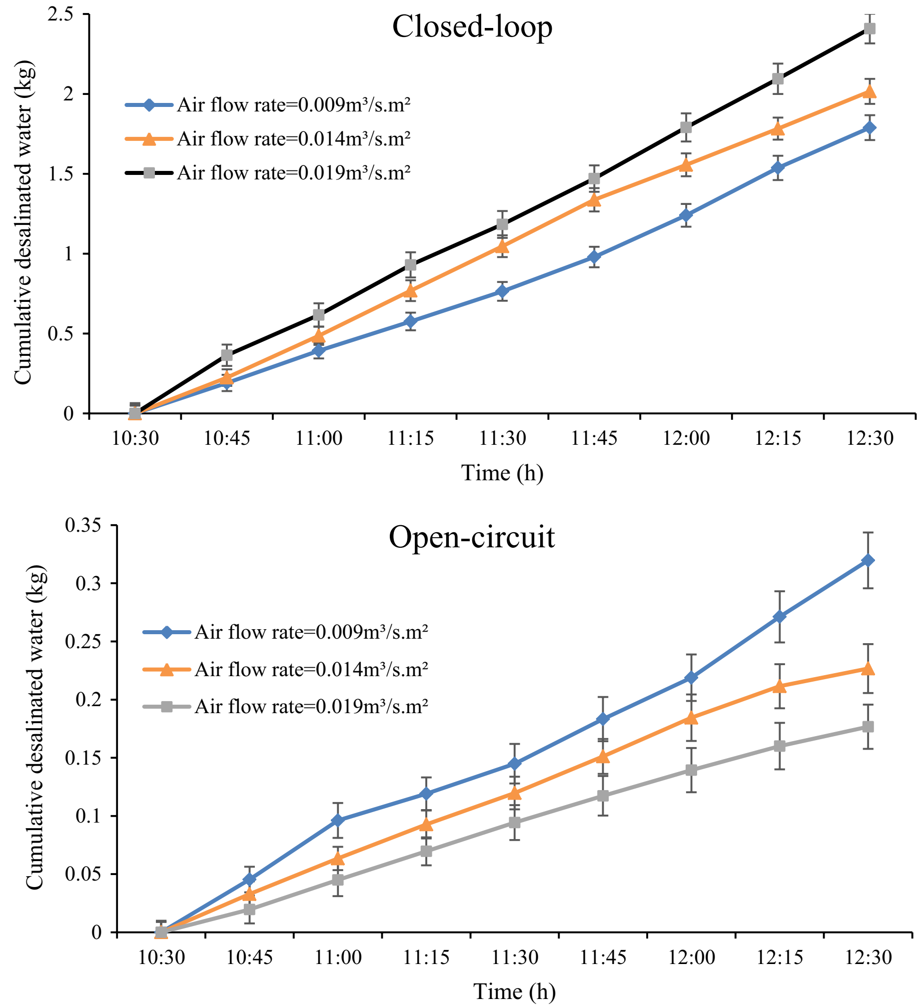

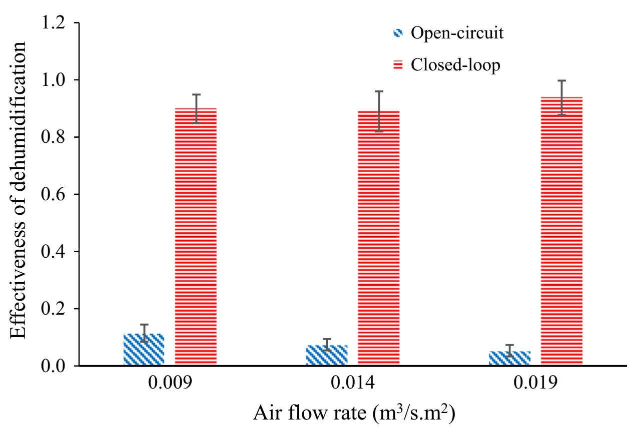

Fig. 9 Effectiveness of dehumidification of the system

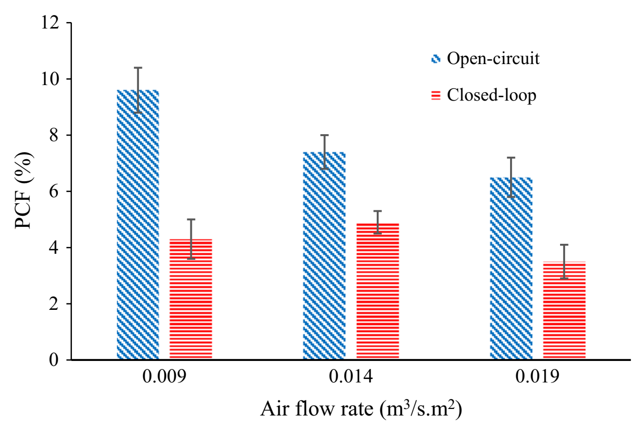

Fig. 10 The pre-condenser fraction at the different operating conditions

- Specific electrical energy consumption ranged between 0.15 and 2.05 kWh/kg.
- Gained output ratio had a significant increment when using the closed-loop compared with the open-circuit air system, and its maximum value was about 2.36.
- The maximum evaporation amount and water productivity were around 1.38 kg and 1 kg/h/m^2 of solar humidifier in the average solar irradiance of 877 W/m^2.

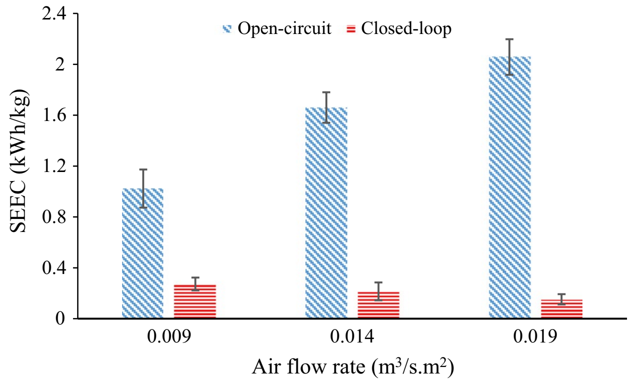

Fig. 11 Specific electrical energy consumption of the system

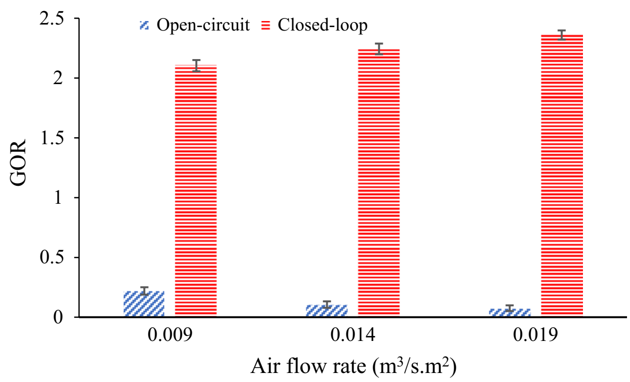

Fig. 12 The effect of the air flow rate and the circulation mode

- Based on the lowest specific electrical energy consumption and the highest water productivity, the air flow rate of 0.019 $m^3/s/m^2$ and the closed-loop air circulation mode is recommended for water desalination by the designed system.

Acknowledgements The authors wish to thank all who assisted in conducting this work.

References

Akhatov ZS, Khalimov A, Saidov KK (2016) A study of the influence of inlet air flow humidity and temperature on thermal efficiency of an evaporation chamber of a solar desalination plant. Appl Sol Energy 52:109–114

Barlow M, Clarke T (2017) Blue gold: the battle against corporate theft of the world's water. Routledge, Abingdon

Bergman TL, Incropera FP (2011) Fundamentals of heat and mass transfer. Wiley, Hoboken

Dehghani S, Date A, Akbarzadeh A (2018) Performance analysis of a heat pump driven humidification–dehumidification desalination system. Desalination 445:95–104. https://doi.org/10.1016/j.desal.2018.07.033

Eid EI, Khalaf-Allah RA, Dahab MA (2018) An experimental study of solar desalination using free jets and an auxiliary hot air stream. Heat Mass Transf 54:1177–1187

El-Agouz SA (2010) A new process of desalination by air passing through seawater based on humidification–dehumidification process. Energy 35:5108–5114. https://doi.org/10.1016/j.energy.2010.08.005

El-Agouz SA, Abd El-Aziz GB, Awad AM (2014) Solar desalination system using spray evaporation. Energy 76:276–283. https://doi.org/10.1016/j.energy.2014.08.009

Elminshawy NAS, Siddiqui FR, Addas MF (2016) Development of an active solar humidification–dehumidification (HDH) desalination system integrated with geothermal energy. Energy Convers Manag 126:608–621. https://doi.org/10.1016/j.enconman.2016.08.044

Elsafi AM (2017) Integration of humidification–dehumidification desalination and concentrated photovoltaic-thermal collectors: energy and exergy-costing analysis. Desalination 424:17–26. https://doi.org/10.1016/j.desal.2017.09.022

El-Said EMS, Kabeel AE, Abdulaziz M (2016) Theoretical study on hybrid desalination system coupled with nano-fluid solar heater for arid states. Desalination 386:84–98. https://doi.org/10.1016/j.desal.2016.03.001

Gao P, Zhang L, Zhang H (2008) Performance analysis of a new type desalination unit of heat pump with humidification and dehumidification. Desalination 220:531–537. https://doi.org/10.1016/j.desal.2007.01.053

Ghazy A, Fath HE (2016) Solar desalination system of combined solar still and humidification–dehumidification unit. Heat Mass Transf 52:2497–2506

Gürtekin E (2019) Experimental and numerical design of renewable-energy-supported advanced biological wastewater treatment plant. Int J Environ Sci Technol 16:1183–1192

Hammadi SH (2018) Theoretical analysis of humidification–dehumidification process in an open type solar desalination system. Case Stud Therm Eng 12:843–851. https://doi.org/10.1016/j.csite.2018.09.009

He WF, Han D, Ji C (2018) Investigation on humidification dehumidification desalination system coupled with heat pump. Desalination 436:152–160. https://doi.org/10.1016/j.desal.2018.02.021

Jamil MA, Zubair SM (2017) On thermoeconomic analysis of a single-effect mechanical vapor compression desalination system. Desalination 420:292–307. https://doi.org/10.1016/j.desal.2017.07.024

Kabeel AE, Hamed MH, Omara ZM, Sharshir SW (2014) Experimental study of a humidification–dehumidification solar technique by natural and forced air circulation. Energy 68:218–228. https://doi.org/10.1016/j.energy.2014.02.094

Lawal D, Antar M, Khalifa A, Zubair S, Al-Sulaiman F (2018) Humidification–dehumidification desalination system operated by a heat pump. Energy Convers Manag 161:128–140. https://doi.org/10.1016/j.enconman.2018.01.067

Liu H, Sharqawy MH (2016) Experimental performance of bubble column humidifier and dehumidifier under varying pressure. Int J Heat Mass Transf 93:934–944. https://doi.org/10.1016/j.ijheatmasstransfer.2015.10.040

Moumouh J, Tahiri M, Salouhi M (2014) Solar thermal energy combined with humidification–dehumidification process for desalination brackish water: technical review. Int J Hydrogen Energy 39:15232–15237. https://doi.org/10.1016/j.ijhydene.2014.04.216

Rahbar N, Esfahani JA (2012) Experimental study of a novel portable solar still by utilizing the heatpipe and thermoelectric module. Desalination 284:55–61. https://doi.org/10.1016/j.desal.2011.08.036

Rahimi-Ahar Z, Hatamipour MS, Ghalavand Y (2018) Experimental investigation of a solar vacuum humidification–dehumidification (VHDH) desalination system. Desalination 437:73–80. https://doi.org/10.1016/j.desal.2018.03.002

Rajaseenivasan T, Shanmugam RK, Hareesh VM, Srithar K (2016) Combined probation of bubble column humidification dehumidification desalination system using solar collectors. Energy 116:459–469. https://doi.org/10.1016/j.energy.2016.09.127

Rostamzadeh H, Namin AS, Ghaebi H, Amidpour M (2018) Performance assessment and optimization of a humidification dehumidification (HDH) system driven by absorption-compression heat pump cycle. Desalination 447:84–101. https://doi.org/10.1016/j.desal.2018.08.015

Santosh R, Arunkumar T, Velraj R, Kumaresan G (2019) Technological advancements in solar energy driven humidification–dehumidification desalination systems—a review. J Clean Prod 207:826–845. https://doi.org/10.1016/j.jclepro.2018.09.247

Sardouei MM, Mortezapour H, Jafari Naeimi K (2018) Temperature distribution and efficiency assessment of different PVT water collector designs. Sādhanā 43:84. https://doi.org/10.1007/s12046-018-0826-x

Sözen A, Öztürk A, Özalp M, Çiftçi E (2018) Influences of alumina and fly ash nanofluid usage on the performance of recuperator including heat pipe bundle. Int J Environ Sci Technol. https://doi.org/10.1007/s13762-018-1832-6

WWAP (2012) The United Nations world water development report 4: managing water under uncertainty and risk, vol 1. UNESCO Paris, Paris

Xu H, Zhao Y, Jia T, Dai YJ (2018) Experimental investigation on a solar assisted heat pump desalination system with humidification–dehumidification. Desalination 437:89–99. https://doi.org/10.1016/j.desal.2018.03.001

Xu H, Zhao Y, Dai YJ (2019) Experimental study on a solar assisted heat pump desalination unit with internal heat recovery based on humidification–dehumidification process. Desalination 452:247–257. https://doi.org/10.1016/j.desal.2018.11.019

Zarzoum K, Zhani K, Bacha HB (2016) Numerical study of a water distillation system using solar energy. J Mech Sci Technol 30:889–902

Zhang Y, Zhu C, Zhang H, Zheng W, You S, Zhen Y (2018) Experimental study of a humidification–dehumidification desalination system with heat pump unit. Desalination 442:108–117. https://doi.org/10.1016/j.desal.2018.05.020

Zhang Y, Zhang H, Zheng W, You S, Wang Y (2019) Numerical investigation of a humidification–dehumidification desalination system driven by heat pump. Energy Convers Manag 180:641–653. https://doi.org/10.1016/j.enconman.2018.11.018

Zondag H, De Vries D, Van Helden W, Van Zolingen R, Van Steenhoven A (2003) The yield of different combined PV-thermal collector designs. Sol Energy 74:253–269